

# Experimental investigation of the displacement flow mechanism and oil recovery in primary polymer flood operations.

MAHON, R., OLUYEMI, G., OYENEYIN, B. and BALOGUN, Y.

2021



## Research Article

# Experimental investigation of the displacement flow mechanism and oil recovery in primary polymer flood operations



Ruissein Mahon<sup>1</sup> · Gbenga Oluyemi<sup>1</sup> · Babs Oyeneyin<sup>1</sup> · Yakubu Balogun<sup>1</sup>

Received: 20 August 2020 / Accepted: 9 February 2021

© The Author(s) 2021 [OPEN](#)

### Abstract

Polymer flooding is a mature chemical enhanced oil recovery method employed in oilfields at pilot testing and field scales. Although results from these applications empirically demonstrate the higher displacement efficiency of polymer flooding over waterflooding operations, the fact remains that not all the oil will be recovered. Thus, continued research attention is needed to further understand the displacement flow mechanism of the immiscible process and the rock–fluid interaction propagated by the multiphase flow during polymer flooding operations. In this study, displacement sequence experiments were conducted to investigate the viscosifying effect of polymer solutions on oil recovery in sandpack systems. The history matching technique was employed to estimate relative permeability, fractional flow and saturation profile through the implementation of a Corey-type function. Experimental results showed that in the case of the motor oil being the displaced fluid, the XG 2500 ppm polymer achieved a 47.0% increase in oil recovery compared with the waterflood case, while the XG 1000 ppm polymer achieved a 38.6% increase in oil recovery compared with the waterflood case. Testing with the motor oil being the displaced fluid, the viscosity ratio was 136 for the waterflood case, 18 for the polymer flood case with XG 1000 ppm polymer and 9 for the polymer flood case with XG 2500 ppm polymer. Findings also revealed that for the waterflood cases, the porous media exhibited oil-wet characteristics, while the polymer flood cases demonstrated water-wet characteristics. This paper provides theoretical support for the application of polymer to improve oil recovery by providing insights into the mechanism behind oil displacement.

✉ Ruissein Mahon, [r.r.mahon@rgu.ac.uk](mailto:r.r.mahon@rgu.ac.uk) | <sup>1</sup>School of Engineering, Robert Gordon University, Aberdeen AB10 7GJ, UK.



SN Applied Sciences

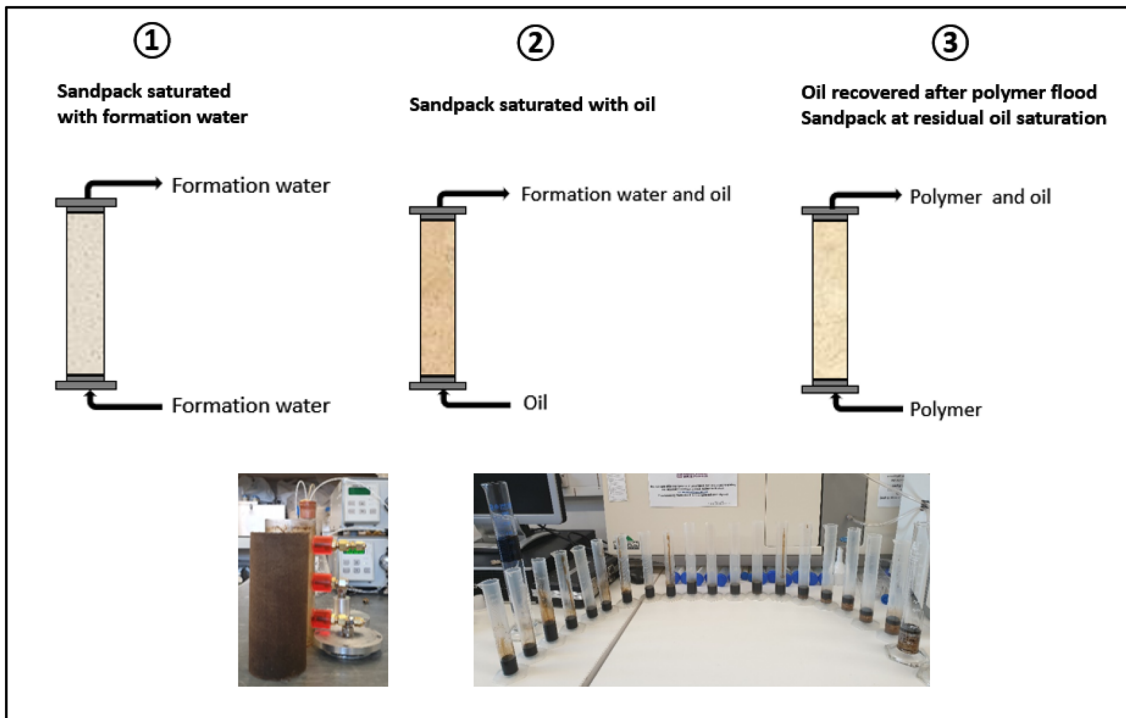
(2021) 3:557

| <https://doi.org/10.1007/s42452-021-04360-7>

Published online: 14 April 2021

SN Applied Sciences  
A **SPRINGER NATURE** journal

**Graphic abstract**



**Highlights**

- The difference in shape of relative permeability curves are indicative of the effect of mobility control of each polymer concentration.
- The water-oil systems exhibited oil-wet characteristics, while the polymer-oil systems demonstrated water-wet characteristics.
- A large contrast in displacing and displaced fluid viscosities led to viscous fingering and early water breakthrough.

**Keywords** Polymer flooding · Relative permeability · Wettability · History matching · Oil recovery

**Nomenclature and acronyms**

**Latin letters**

A	Cross-sectional area of the porous media
BHP	Bottomhole pressure
EnKF	Ensemble Kalman filter
EOR	Enhanced oil recovery
HPAM	Partially hydrolysed polyacrylamide
HTHS	High temperature and high salinity
IFT	Interfacial tension
JBN	Johnson–Bossler–Neumann
K	Permeability of porous media
$k_{ro}^0$	Oil relative permeability endpoint
$k_{ro}$	Oil relative permeability
$k_{rw}$	Water relative permeability
$k_{rw}^0$	Water relative permeability endpoint
L	Length of the porous media
LM	Levenberg–Marquardt

L-BFGS	Broyden–Fletcher–Goldfarb–Shanno
$N_o$	Corey-type oil shape factor
$N_w$	Corey-type water shape factor
OOIP	Original oil in place
PV	Pore volume
Q	Volumetric flowrate
RF	Resistant factor
RRF	Residual resistant factor
$S_o$	Oil saturation
$S_{or}$	Residual oil saturation
$S_w$	Water saturation
$S_w^*$	Normalised water saturation
$S_{wi}$	Irreducible water saturation
SCAL	Special core analysis
TDS	Total dissolved solids
USS	Unsteady state
XG	Xanthan gum

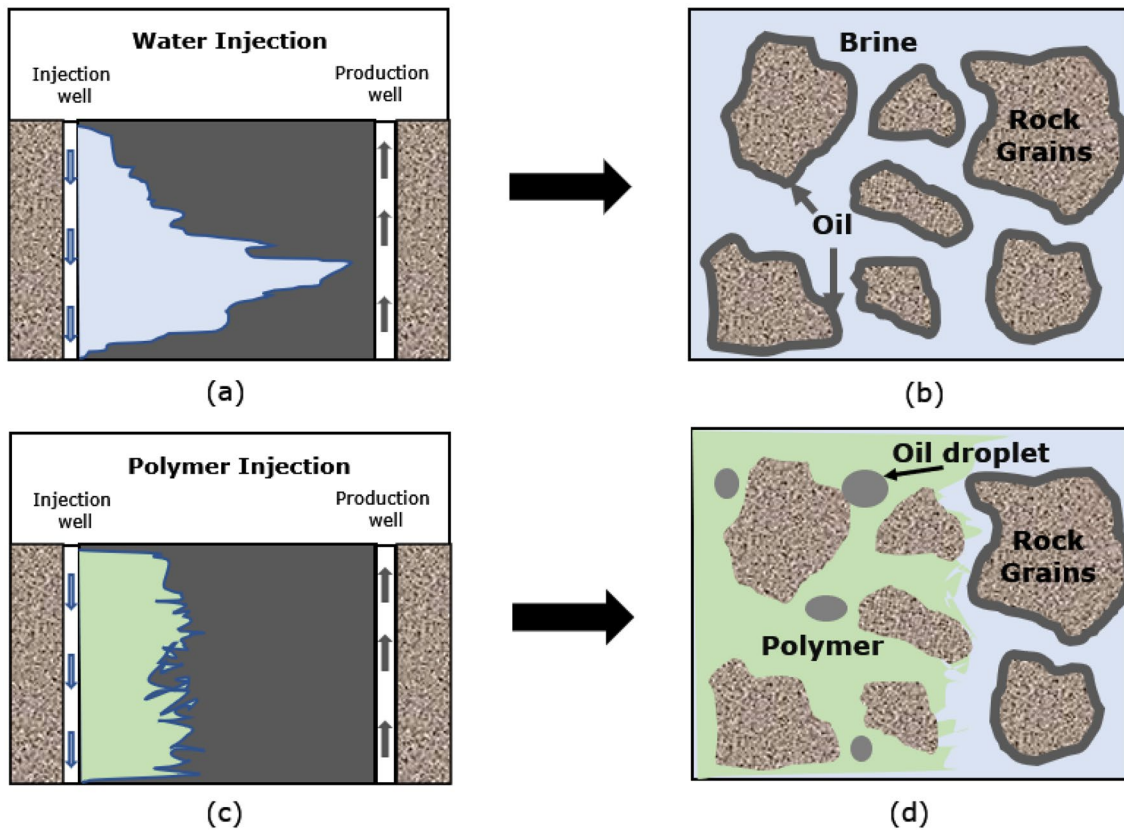


**Fig. 1** Application of EOR techniques demonstrating mobility control and wettability alteration: **a** waterflood operation with viscous fingering, **b** oil-wet wettability condition, **c** polymer flood operation with a stable front and **d** water-wet wettability condition

#### Greek letters

$\mu$	Fluid viscosity
$\Phi$	Porosity

## 1 Introduction

Global energy consumption is projected to rise by approximately 20% relative to current consumption levels by 2040 [1]. Although there will be significant future changes in the global energy mix in terms of renewable and non-renewable sources of energy, oil will continue to play a key role in the global energy portfolio. Approximately only one-third of oil present in reservoirs can be economically produced after secondary recovery [2]. As such, enhanced oil recovery (EOR) methods serve a useful purpose in helping to develop hydrocarbon oil reserves. Polymer flooding operations have emerged as one of the most promising EOR techniques to increase ultimate oil recovery [3]. Theoretical evidence shows that polymers can significantly increase the viscosity of a fluid and reduce the water/oil-mobility ratio, thus improving the volumetric sweep efficiency and ultimate oil recovery [4, 5]. In this regard, the

modelling of oil production by polymer flooding requires a comprehensive understanding of rock–fluid interaction for oilfield applications since polymer flooding is becoming more extensively implemented not only for pilot tests but also at the field scale operational level [6–9].

In EOR operations, good mobility control can be achieved when the viscosity of the injected fluid is higher than the viscosity of the oil in the reservoir driving the oil from the injection well to the production well by means of a piston-like displacement effect [10]. Conversely, poor mobility control due to a lower viscosity of the injected fluid can result in severe viscous fingering and low oil recoveries. Figure 1 illustrates the mechanisms at play in waterflood and polymer flood operations. At the macroscopic scale for waterflood operations, there exist the tendency of water fingers forming in the oil zone, leading to early breakthrough and reduced sweep efficiency (Fig. 1a). However, for polymer flood operations, this fingering effect is not present, and a stable fluid front (polymer) is formed resulting in increased sweep efficiency (Fig. 1c). At the microscopic scale, after waterflooding, an oil layer adheres to the surface of the rock grains demonstrating an oil-wet characteristic (Fig. 1b). After polymer flooding, the

wettability of the porous media changes to a water-wet characteristic with the oil layer no longer adhering to the rock grain (Fig. 1d).

Several polymer flood studies have been conducted using experimental, numerical simulation and field methods to better understand the polymer displacement mechanism. Firozjahi et al. [5] experimentally and numerically investigated the difference in performance of polymer floods using co-polymer Zetag 8187G and waterfloods under high temperature and high salinity (HTHS) conditions. The rheological behaviour of the polymer showed that by increasing temperature and salinity, the viscosity of the polymer solution provided a stable polymer front despite a decrease in viscosity. Experimental results showed that under HTHS conditions, the waterflood experiment recovered 33.68% of the original oil in place (OOIP), whereas the polymer flood recovered 60.95% of the OOIP. Thus, a 27.27% increase was derived under HTHS conditions. The resistant factor (RF) and residual resistant factor (RRF) were found to be 5.01 and 1.39, respectively. Delamaide et al. [7] studied the characteristics of primary, secondary and tertiary polymer floods in a heavy oil field. Results revealed that the primary polymer flood resulted in the maintenance of a relatively constant oil rate with water cut remaining low. The secondary polymer flood resulted in increased reservoir pressure and oil rate without reaching a high water cut (over 50%). The tertiary polymer flood resulted in a good pressure response and increased oil rate, but with oil production at high water cut. Schneider and Owens [11] performed displacement sequence experiments using hydrolysed polyacrylamide to simulate polymer flooding after waterflood operations in core samples. To evaluate the level of incremental recovery and economics of prior polymer slug injection, polymer-oil relative permeability data were used in performance evaluation calculations. Results showed that rock wettability is responsible for the effects of polymer floods, and relative permeability curves were developed using the Johnson–Bossler–Neumann (JBN) method. The adsorbed polymer layer increased the oil relative permeability and decreased the residual oil saturation. These studies show that while polymer flood operations at both the laboratory and field scale have resulted in increased oil production, the accurate estimation of the multiphase flow parameters used to model and evaluate the displacement flow mechanism in polymer flooding is critical to its successful application. Knowledge of the multiphase flow parameters and a comprehensive understanding of the interaction between them are used to evaluate the probabilities of improved hydrocarbon recovery and economics and as performance evaluation indicators. A detailed summary of polymer flooding studies conducted using different methods and their findings are provided in Table 1.

Relative permeability, the ratio of the effective permeability of a particular fluid at a specific saturation to the absolute permeability of that fluid at 100% saturation, is a key multiphase flow parameter [18]. Relative permeability is dependent upon factors such as temperature, wettability, fluid properties (density and viscosity), interfacial tension, injection rate, time and rock properties (permeability and pore size distribution) [19–21]. Accurate relative permeability curves of polymer flooding are required to predict hydrocarbon production and to design injection and production programmes. Generally, relative permeability curves are estimated using two methods, the steady-state (SS) and unsteady-state (USS) method. The SS method requires that both the oil and water phases reach equilibrium, which can be time-consuming with an associated high probability of experimental errors. The USS method takes less time and is operationally simpler; however, the JBN method that is used in the USS method suffers from several simplifying assumptions and is unable to capture the effects of polymer diffusion and adsorption.

Several numerical methods have been used by different investigators to estimate relative permeability; however, the majority of these numerical methods proposed have been for water–oil systems. Liu et al. [22] combined a numerical simulation model of polymer flooding with the Levenberg–Marquardt (LM) algorithm to develop an inversion method to estimate relative permeability values in polymer flooding. Effects of polymer adsorption, diffusion, viscosity and residual resistance were incorporated into the proposed method and the accuracy of these input parameters having a significant effect on the inversed relative permeability curve. Hou et al. [23] applied the LM algorithm to perform automatic history matching to optimise the production performance and relative permeability curves. Results show that the relative permeability of oil is sensitive to cumulative production data of the producer well, whereas the relative permeability of water is sensitive to the bottomhole pressure (BHP) data of the injector well. Schembre and Kovscek [24] conducted automatic history matching of imbibition experimental data employing the annealing-optimisation method and developed the corresponding means to determine the relative permeability and capillary pressure values. They found that non-equilibrium effects detected at laboratory scale influence the estimation of USS relative permeability and capillary pressure resulting in the inaccurate assessment of multiphase flow properties. A detailed summary of the different numerical methods proposed by different investigators to estimate relative permeability are provided in Table 2.

These studies elucidate the fact that in terms of relative permeability, much research focus has been on waterflood scenarios (water–oil systems) with far less attention given to polymer flood scenarios (polymer-oil

**Table 1** Studies of polymer flooding

Investigator	Method	Displacing fluid	Study findings
Abirov et al. [12]	Experimental	Associative polymer and partially hydrolysed polyacrylamide (HPAM)	Using brine and HPAM, investigated the displacement of low viscosity oil. Experiments conducted at 82 °C and brine salinity of 92,000 ppm revealed that associative polymer is more stable than HPAM, having a secondary oil recovery of 6.52%. The associative polymer was recommended for pilot testing at reservoir scale
Al-Shakry et al. [13]	Experimental	HPAM—Type A HPAM—Type B	Investigated the in situ rheological behaviour of HPAM with and without the presence of oil under different wettability and pre-treatment conditions to optimise polymer injectivity. Found that the presence of oil significantly influences polymer rheology and that polymer pre-shearing changes the viscoelastic properties of the polymer. Results also showed that aged cores had better polymer injectivity, whereas polymer injectivity was underestimated in cores with 100% $S_w$
Song et al. [14]	Experimental	Polyacrylamide-based polymer	Studied the disproportionate effects of polymer on the relative permeability of gas and water in fractured-shale reservoirs. Results revealed that the reduction of water relative permeability can be attributed to the polymer and is more that of the gas relative permeability. Polymer treatment was found not to impair gas flow in wide fractures
Fabbri et al. [15]	Experimental	HPAM 3630S	Interpreted three tertiary polymer floods using an in-house simulator. Identified a memory effect through quantitative analysis of the X-ray saturation maps of the secondary drainage relative permeability, attributing it to a hysteresis phenomenon. Developed a hysteresis model which uses two additional matching parameters based upon the assumption that the rock and fluids behave as an oil-wet system
Lopez and Blunt [16]	Numerical simulation	Xanthan polymer	Used a pore-network model to investigate the effects of the non-Newtonian rheological property of polymer on the relative permeability. Results indicated that as the pressure gradient was applied, the oil relative permeability does not significantly change whereas the relative permeability of the non-Newtonian phase initially decreases before increasing, lower than the Newtonian values
Barreau et al. [17]	Experimental and numerical	Polyacrylamide (PAM)	Performed unsteady-state (USS) two-phase flow experiments to investigate the effect of PAM polymer on relative permeability and capillary pressure in core samples. Assumed that the PAM polymer was uniformly adsorbed on the rock surface and obtained the relative permeability curve using the USS method. Results showed that the PAM polymer flood increased the irreducible water saturation and significantly decreased the water relative permeability but had negligible effects on the oil relative permeability

systems). However, examining polymer flood scenarios is important in evaluating the potential magnitude of improved oil recovery and economics. For this reason, there is a need for polymer-oil relative permeability data

for use in performance evaluation calculations. This study helps to fill this gap by performing sandpack displacement sequence experiments to examine the viscosifying effect of polymer solutions on oil recovery under ambient

**Table 2** Numerical methods proposed by different investigators to estimate relative permeability

Investigator	Numerical methods	Study findings
Fayazi et al. [25]	Genetic algorithm	Used an automated history matching algorithm which implements B-spline approximations to represent relative permeability curves. The algorithm can be extended to improve the accuracy of modelled production data from oil reservoirs. Recommended that the pseudo functions for coarse grid simulation be used to achieve better results
Zhang et al. [26]	Damped iterative ensemble Kalman filter (IEnKF) algorithm	Implemented an (IEnKF) algorithm to estimate relative permeability and capillary pressure by history matching waterflood experimental data. Results showed that the relative permeability of water was estimated more accurately than the relative permeability of oil and capillary pressure. This was attributed to the preferential sensitivity of the experimental data
Zhang and Yang [27]	Ensemble Kalman filter (EnKF) method	Proposed an ensemble-based technique (EnKF method) by history matching measurement data and estimated relative permeability and capillary pressure values. A reasonably good match was found between the updated and reference production history profiles. The proposed technique demonstrated good computational efficiency and uncertainty analysis
Li et al. [28]	EnKF method	Implemented an ensemble-based technique (EnKF method) to estimate three-phase relative permeability values by history matching production data. The endpoints and shape factors of the relative permeability curves were reasonably estimated using this method based upon history matching with production data
Eyidinov et al. [29]	Broyden–Fletcher–Goldfarb–Shanno (BFGS)	Used the limited-memory Broyden–Fletcher–Goldfarb–Shanno (L-BFGS) algorithm and proposed a numerical inversion method to simultaneously estimate relative permeability, porosity and absolute permeability. Concluded that uncertainty in model parameters and reservoir performance prediction can be reduced by conditioning production data
Sun and Mohanty [30]	Genetic algorithm	Applied a genetic algorithm for optimisation and built an automated fitting method of relative permeability curves. Results showed that at low injection rates, the match between the simulation and experimental data was reasonably good while for higher injection rates, the genetic algorithm did not converge to attain its global optimum
Giller et al. [31]	Artificial neural network	Developed a model algorithm to predict the relative permeability by fitting core-flood data with the artificial neural network method which incorporates the controlling mechanisms and parameters into the model. The proposed model exhibited sensitivity to several reservoir properties, and the accuracy of the estimated relative permeability values at residual saturations was improved by using normalised saturations
Yang and Watson [32]	Bayesian estimation method	Implemented a Bayesian type performance index that incorporates reservoir production data and laboratory estimates of relative permeability values into an automatic history-matching algorithm. The methodology was tested with hypothetical waterflood data and performed reasonably well

laboratory conditions. Relative permeabilities, fractional flows and saturation profiles are estimated through the history matching technique using the LM method for both water–oil and polymer–oil systems to evaluate and compare their performances. The effect of wettability alteration is inferred from the crossover saturations of the relative permeability curves to provide insight on how this phenomenon can lead to a further favourable displacement condition.

## 2 Theoretical background of relative permeability calculation method

Obtaining reliable relative permeability curves from core or sandpack experiments is critical in the characterisation of oil and gas reservoirs and in the estimation of their production capabilities. Relative permeability is not a directly measurable property of the rock but is estimated from measured data utilising mathematical models of the

physical phenomena. This process is known as inverse modelling. Using the data measured during displacement experiments, the estimates of relative permeability functions can be obtained and is referred to as the inverse problem.

## 2.1 Relative permeability calculation technique: Unsteady-state method

During the USS method, displacement of one fluid phase by another immiscible fluid phase takes place and can be characteristic of the multiphase flow behaviour in reservoirs [33, 34]. The USS relative permeability measurements are simpler than the SS methods with the measured variables being time dependent. Relative permeability estimations can be made using either explicit or implicit methods. The explicit methods commonly used are the JBN method [35] based on the Buckley–Leverett theory and the modified graphical version by Jones and Roszelle (JR) method [36]. The implicit or history matching method is based on numerical calculation. During the history matching procedure, the relative permeability parameters are adjusted to match the differential pressure and cumulative production data from the core flooding experiments [34].

History matching is an inverse modelling process whereby pressure and production data measured from displacement experiments at given time intervals, referred to as history data is matched with simulated data with the input parameter values updated. In this process, the input parameter values are verified or updated by measuring the disagreement between the historical data and simulated data. The history data is compared with the simulated data, and if there exists an error above the set tolerance, a parameter in the simulation model is adjusted and new simulation data generated. The process is repeated until the tolerance between the historical data and simulated data is achieved [18].

## 2.2 Formulation of parameter estimation and solution

The commercial simulator used in this work to perform the history matching was Sendra. It is a 1D black oil simulation model used for analysing special core analysis (SCAL) experiments and can estimate relative permeability and capillary pressure data from multiphase flow experiments.

The constrained minimisation problem is solved by the parameter estimator:

$$\text{Minimise } (Y - F(\beta))^T W (Y - F(\beta)) \quad (1)$$

$$\text{Subject to } G\beta > h \quad (2)$$

where  $Y$  is the vector of experimental results,  $F(\beta)$  is the vector of simulated results, and  $\beta$  is the vector of parameters to be estimated.  $W$  is a diagonal weighting matrix where each entry is set to the variance of the experimental data. The linear inequality constraints on the vector parameters  $\beta$  are established using the matrix  $G$  and the vector  $h$ , allowing either a parameter to be bounded in a finite interval or be bounded by other parameters.

The parameter estimation problem is solved using the LM method with modifications made to cater for linear constraints and the derivatives of  $F(\beta)$  being approximated with forward or central differences [37].

## 2.3 Empirical relative permeability correlation

There are several empirical relative permeability correlations within the literature, including Corey correlation [38], Sigmund and McCaffery correlation [39], LET correlation [40], Burdine correlation [41] and Chierici correlation [42]. During the history matching process, the Corey correlation, Sigmund and McCaffery correlation and LET correlation were implemented with the Corey-type analytical function providing the best match for all cases.

Corey's correlation has been extensively used by researchers as it is relatively simple and easy to use. Among its advantages is the fact that it can fit relative permeability data points, describing the shape of each curve with an exponent value [43]. The power law function assumes that the water and oil phase relative permeabilities are independent of the saturation of the other phase [44]. The relative permeabilities of the Corey-type analytical correlation are defined in Eq. (3) and Eq. (4):

$$k_{rw} = k_{rw}^0 (S_w^*)^{N_w} \quad (3)$$

$$k_{ro} = k_{ro}^0 (1 - S_w^*)^{N_o} \quad (4)$$

where  $S_w^*$  denoted by Eq. (5)

$$S_w^* = \frac{S_w - S_{wi}}{1 - S_{wi} - S_{or}} \quad (5)$$

where  $k_{rw}$  is the water relative permeability,  $k_{ro}$  is the oil relative permeability,  $k_{rw}^0$  is the water relative permeability endpoint,  $k_{ro}^0$  is the oil relative permeability endpoint,  $S_w^*$  is the normalised water saturation,  $S_w$  is the water saturation,  $S_{wi}$  is the irreducible water saturation and  $S_{or}$  is the residual oil saturation.  $N_w$  and  $N_o$  are the water and oil Corey-type parameters, which influence the shape of the water and oil relative permeability curves.

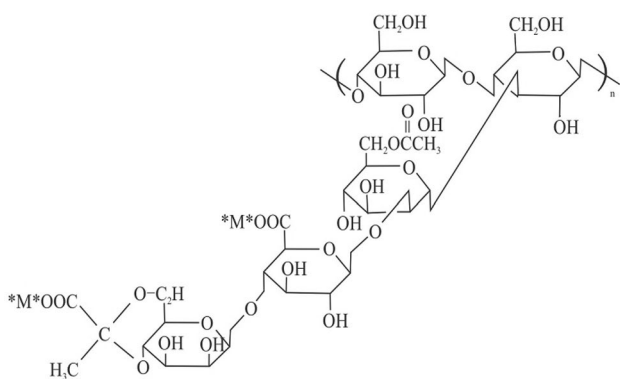


Fig. 2 Structure of xanthan gum [45]

### 3 Experimental method

#### 3.1 Materials

##### 3.1.1 Fluid properties

In this study, six fluid systems were used, formation water, seawater, XG 1000 ppm, XG 2500 ppm, heavy oil blend and motor oil.

**3.1.1.1 Xanthan gum solutions** The xanthan gum used to prepare the polymer solutions was supplied by Mi SWACO with a 98% purity, having a molecular weight between 2 and 2.5 million Daltons. Figure 2 shows the chemical structure of xanthan gum. The xanthan solutions were prepared by slowly adding the polymer powder into tap water preventing the formation of “fish-eyes” during the mixing process. Thereafter, the polymer solutions were

Table 3 Xanthan solution properties at 22 °C

Fluid properties	XG 1000 ppm	XG 2500 ppm
Density (kg/m <sup>3</sup> )	1007.7	1018.5
Viscosity (cP)	7.8	14.7

thoroughly mixed, becoming transparent in appearance. The polymer solutions were sheared at different shear rates under ambient conditions (22 °C) using a Fann 35SA viscometer. The polymer concentrations used in this study were 1000 ppm and 2500 ppm (XG 1000 ppm and XG 2500 ppm). Figure 3 shows the viscosity and shear stress flow curves of the polymer solutions (XG 1000 ppm and XG 2500 ppm), and Table 3 presents the density and viscosity properties of the polymer solutions. The 510 s<sup>-1</sup> shear rate (300 rpm) viscosity values of the polymer solutions were used within this study to perform history matching using the commercial simulator Sendra, to operate under the same condition across all cases.

**3.1.1.2 Oil samples** The two oil samples used in this study were: (1) motor oil (Granville HYPALUBE Mineral 10 W/30) and (2) heavy oil blend. The heavy oil blend was a mixture of heavy oil and kerosene having a proportion of 70% heavy oil and 30% kerosene. Figure 4 shows the viscosity and shear stress flow curves of the motor oil and heavy oil blend, and Table 4 presents the oil density and viscosity properties. Similarly, the 510 s<sup>-1</sup> shear rate (300 rpm) viscosity values of the oil samples were used within this study to perform history matching using the commercial simulator Sendra, to operate under the same condition across all cases.

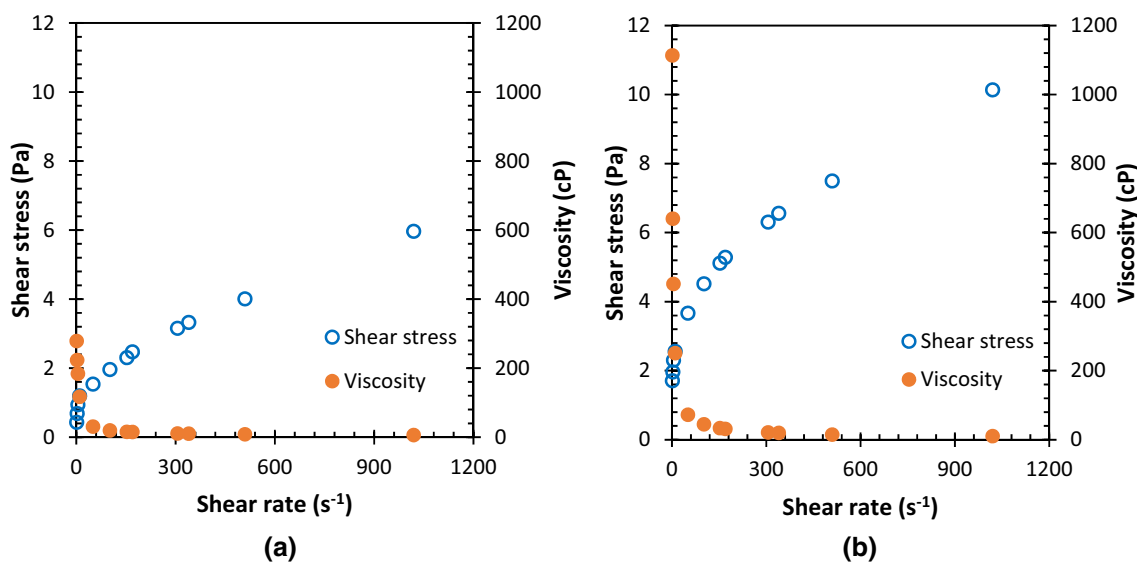


Fig. 3 Shear stress and viscosity flow curves of a XG 1000 ppm and b XG 2500 ppm

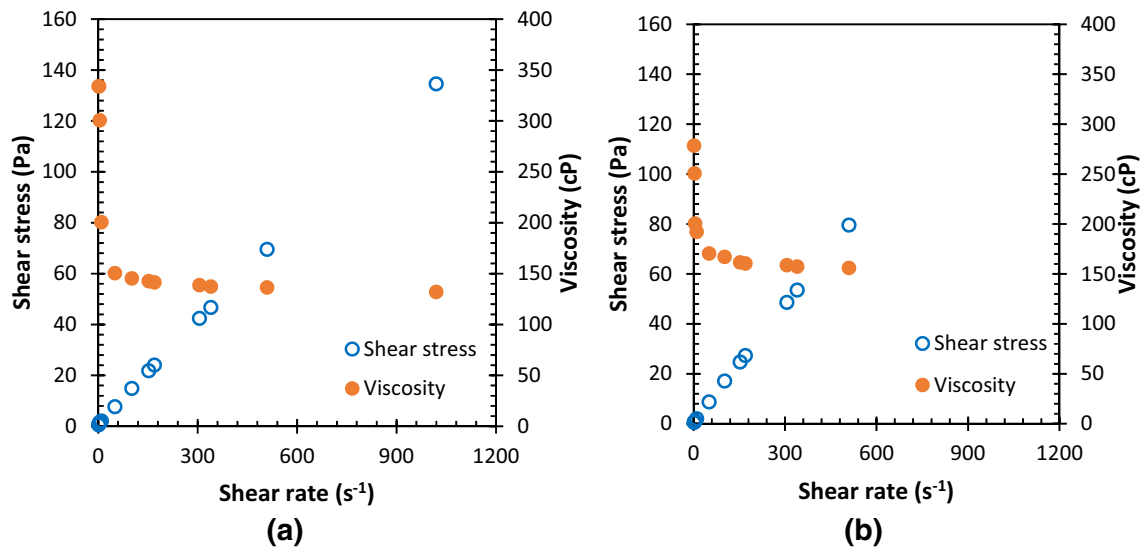


Fig. 4 Shear stress and viscosity flow curves of **a** motor oil and **b** heavy oil blend

Table 4 Oil properties at 22 °C

Fluid properties	Motor oil	Heavy oil blend
Density (kg/m <sup>3</sup> )	874.4	890.0
Viscosity (cP)	136.3	156.0

**3.1.1.3 Synthetic brines** The two synthetic brines used in this study were: (1) formation water and (2) seawater. The formation water was prepared to mimic the fluid within the porous media (to set up the initial fluid saturation condition of the sandpacks) before flooding operations, whereas the seawater was used as one of the displacing fluids within the flooding operations. The synthetic brines were prepared using deionised water and dissolving different analytical grade salts. The salts used were sodium

chloride (NaCl), calcium chloride anhydrous (CaCl<sub>2</sub>), magnesium chloride (MgCl<sub>2</sub>), calcium carbonate (CaCO<sub>3</sub>), sodium sulphate (Na<sub>2</sub>SO<sub>4</sub>), sodium hydrogen carbonate (NaHCO<sub>3</sub>), potassium chloride (KCl) and magnesium chloride hexahydrate (MgCl<sub>2</sub>·6H<sub>2</sub>O). To remove any precipitate within the synthetic brines, the solutions were filtered with 0.22-µm laboratory-grade filter paper. Table 5 shows the chemical composition of the synthetic brines.

**3.1.2 Rock properties**

The porous media used in this study were sandpacks consisting of unconsolidated silica sand having a 40/60 mesh size. Mechanical sieve analysis was performed on a sample of the 40/60 silica sand used in this study; the grain size distribution of the 40/60 silica sand is shown in Fig. 5. The

Table 5 Chemical composition of formation water and seawater samples

Composition	Concentration (ppm)	
	Seawater	Formation water
NaCl	140,316	26,400
CaCl <sub>2</sub>	40,287	1180
MgCl <sub>2</sub>	2856	–
CaCO <sub>3</sub>	1628	–
Na <sub>2</sub> SO <sub>4</sub>	2588	–
NaHCO <sub>3</sub>	2016	7340
KCl	–	400
MgCl <sub>2</sub> ·6H <sub>2</sub> O	–	5270
Total	189,691	40,590

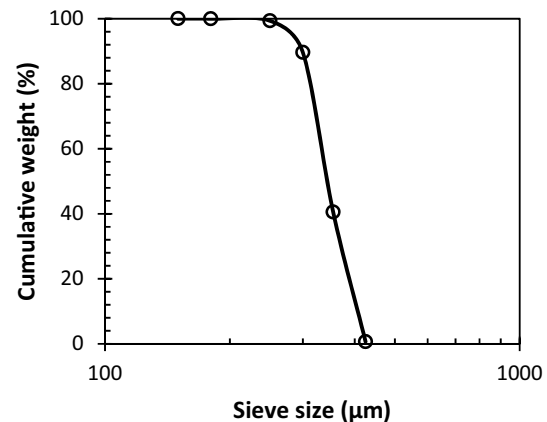
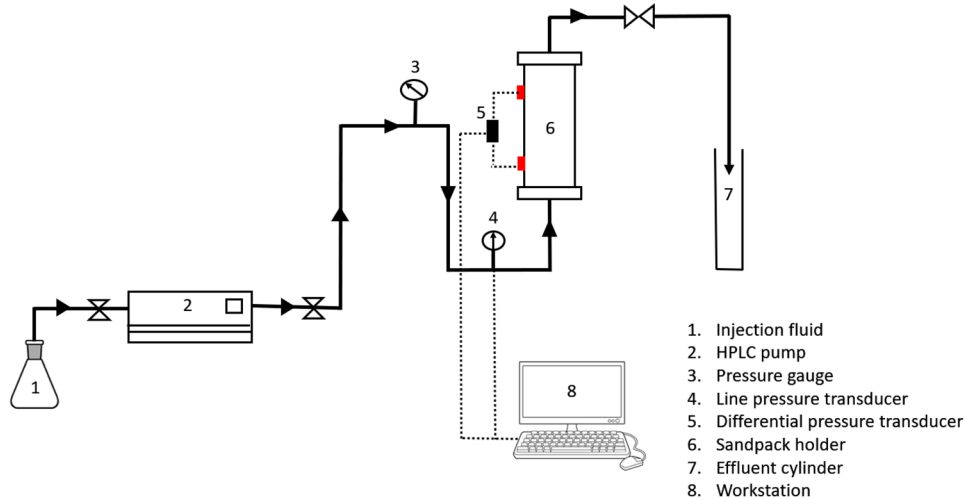


Fig. 5 Grain size distribution of the 40/60 silica sand

**Fig. 6** Schematic of sandpack flow loop



values of  $d_{10}$ ,  $d_{50}$  and  $d_{90}$  of the 40/60 silica sand are 400  $\mu\text{m}$ , 340  $\mu\text{m}$  and 300  $\mu\text{m}$ , respectively.

### 3.2 Experimental setup

A schematic of the experimental setup used in this study is shown in Fig. 6. The sandpack holder used in this study is made up of two endcaps, two distributors, two rubber O-rings and an acrylic tube sand holder. The sandpack holder is 17 cm in length and 6.5 cm in diameter. A 200-mesh screen was placed on the endcap/distributor to prevent sand flowing out of the sandpack. Two rubber O-rings in the two endcaps sealed the endcaps when connected to the acrylic tube sand holder. The pumping apparatus used was a high-performance liquid chromatography (HPLC) dual-piston pump. All fluids were injected into the sandpack using this pump. The production fluid was collected in the effluent cylinder at specific time intervals. The data acquisition system used consisted of a pressure gauge, line pressure transducer and differential pressure transducer (Omega), a signal conditioning and analog-to-digital converter device (NI 9212) and workstation with LabVIEW installed.

### 3.3 Experimental procedure

#### 3.3.1 Sandpack preparation and property determination

Before each flow test, the sandpack holder was thoroughly cleaned with 99% ethanol and then rinsed with water. For each flow test, fresh 40/60 silica sand was vertically packed in a stepwise manner using a sieve shaker to evenly distribute the silica sand into the sandpack holder to ensure homogeneity for all the tests, thus preventing preferential flow paths. The sandpack holder was vibrated for approximately 20 min to ensure as tight as possible sandpack.

After the sandpack was filled with the desired silica sand, it was saturated with formation water. For each sandpack, the porosity ( $\phi$ ) and pore volume (PV) were both calculated using the weight method. The PV was calculated from the difference between the bulk volume and grain volume, while the porosity was calculated from the ratio of the PV to the bulk volume of the sandpack holder. After the pore volume and porosity of the sandpack were determined, the sandpack was saturated with formation water and then connected as shown in Fig. 6 and further saturated with formation water at a flowrate of 1.0 mL/min to determine the absolute permeability of the sandpack using Darcy’s law. The pressure drop between the two transducer ports with a length of 15 cm was recorded using the data acquisition system.

After the absolute permeability was determined, the sandpack was saturated with oil at an injection rate of 1.0 mL/min. Effluent samples were collected and measured during the injection; when no more water was produced as seen in the effluent, the remaining water in the sandpack was determined to be irreducible, and the irreducible water saturation was calculated as the difference between the volume of water saturating the sandpack and that produced during the oil injection. After the

**Table 6** Overview of petrophysical parameters of sandpacks used in this study

Sandpack	Absolute permeability (D)	Pore volume ( $\text{cm}^3$ )	Porosity (%)	Irreducible water saturation (%)
SP1-30-09	5.0	166.9	33.5	15.5
SP2-28-10	5.0	163.3	32.8	14.3
SP9-16-12	5.5	173.1	34.8	13.4
SP7-02-12	4.8	163.5	32.9	14.4
SP8-09-12	5.0	173.8	34.9	13.7
SP10-18-12	6.0	166.6	33.4	15.5

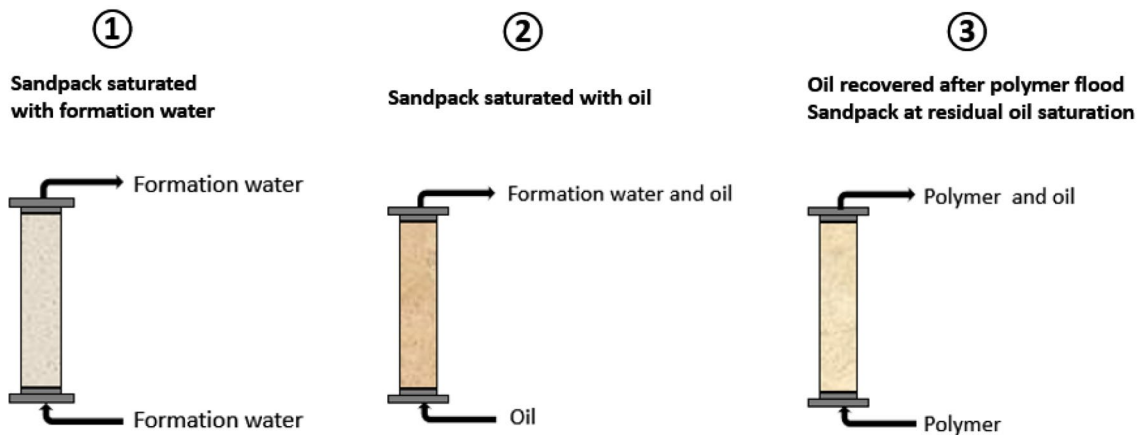


Fig. 7 Schematic of experimental flood procedure

initial water saturation of the sandpack was determined, the sandpack initialisation had occurred (the sandpack mimicked an oil reservoir in terms of reservoir fluid saturation distributions).

The absolute permeability, pore volume, porosity and initial water saturation of the six sandpacks used in this study are summarised in Table 6. The porosity values of the sandpacks were found to be in close range, between 32.8 and 34.9%, indicating that a consistent packing procedure was followed resulting in reliable pore volumes having a range between 163.3 and 173.8 cm<sup>3</sup>. The absolute permeability range of the sandpacks were between 4.8 and 6.0 D and irreducible water saturation ranging from between 13.4 and 15.5%. The close property ranges of the sandpacks reflects their reasonably good homogeneity.

### 3.3.2 Polymer flooding procedure

Figure 7 shows a schematic of the experimental flooding procedure. After the sandpack preparation, the polymer injection proceeded at a flowrate of 1.0 mL/min. The pressure at the production end was atmospheric pressure, and the time-dependent injection pressure and associated cumulative oil and polymer production were recorded at different time intervals. Polymer injection was continued until the oil production became negligible. The residual oil saturation to polymer was then calculated as the difference between the volume of oil saturating the sandpack and cumulative oil produced during polymer injection. Water injection displacement experiments were also conducted and used as a baseline to provide a representative comparison with the polymer floods at different concentrations.

## 4 Results and discussion

For the six sandpack flood experiments performed in this study, the effect of displaced fluid and displacing fluid viscosities were investigated in terms of residual oil saturation, oil recovery, relative permeability, fractional flow and saturation profiles. Also, the effect of wettability alteration was inferred using the relative permeability curves.

### 4.1 Residual oil saturation and oil recovery

Table 7 presents the residual oil saturation for the various sandpacks. For both cases where the displaced fluid was motor oil or heavy oil blend, the residual oil saturation at the end of the waterfloods was higher than at the end of the polymer flood experiments. This may be attributed to the capillary forces within the pore spaces of the porous media and the viscosity ratio. Hence, as the displacing fluid viscosity increases, the residual oil saturation decreases resulting in increased oil recovery.

Figure 8 shows images of two sandpacks (a and c) after polymer flooding operations and production of heavy oil blend and motor oil (b and d) over time.

Figure 9 shows the oil recovery of the different floods using motor oil and heavy oil blend as the displaced fluid

Table 7 Residual oil saturation for the different sandpacks

Sandpack	Displaced fluid	Displacing fluid	Residual oil saturation (%)
SP1-30-09	Motor oil	XG 2500 ppm	18
SP2-28-10	Motor oil	XG 1000 ppm	25
SP9-16-12	Motor oil	Sea water	30
SP7-02-12	Heavy oi blend	XG 2500 ppm	15
SP8-0912	Heavy oil blend	XG 1000 ppm	17
SP10-18-12	Heavy oil blend	Sea water	26

**Fig. 8** Sandpack and production effluent samples for different displaced fluids **a, b** heavy oil blend and **c, d** motor oil



(a)



(b)



(c)



(d)

and XG 2500 ppm, XG 1000 ppm and seawater as the displacing fluid. The viscosity of the displacing fluid impacts the resulting oil recovery profile. Figure 9a presents the cases of the motor oil being the displaced fluid; the displacing fluid being XG 2500 ppm resulted in the highest overall oil recovery of 72.3%, while the seawater being the displacing fluid resulted in the lowest oil recovery of 25.3%. Thus, the XG 2500 ppm polymer achieved a 47.0% increase in oil recovery compared with the waterflood and the XG 1000 ppm polymer achieved a 38.6% increase in oil recovery compared with the waterflood for the scenarios with the motor oil being the displaced fluid. While a similar

trend was observed to the motor oil cases (Fig. 9b), the case of the heavy oil blend being the displaced fluid shows the decreasing ability of the high-viscosity displacing fluid to mobilise the heavy oil blend in the sandpack. This is a result of the less favourable viscosity ratio and consequently reduction in oil recovery factor. The displacing fluid, XG 2500 ppm, again resulted in the highest overall oil recovery of 62.1%, while the seawater as the displacing fluid again resulted in the lowest oil recovery of 17.3%. Hence, the XG 2500 ppm polymer achieved a 44.8% increase in oil recovery compared with the waterflood and the XG 1000 ppm polymer achieved a 30.7% increase in oil

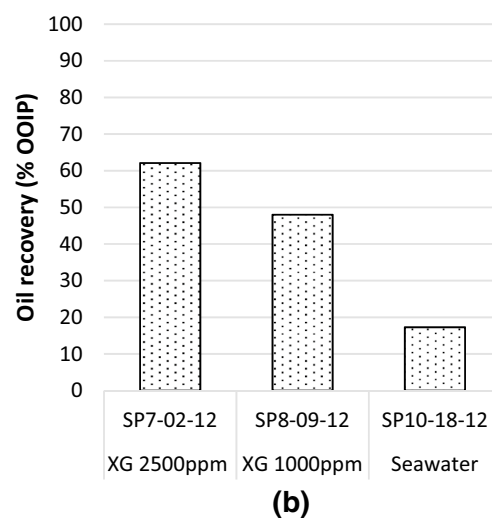
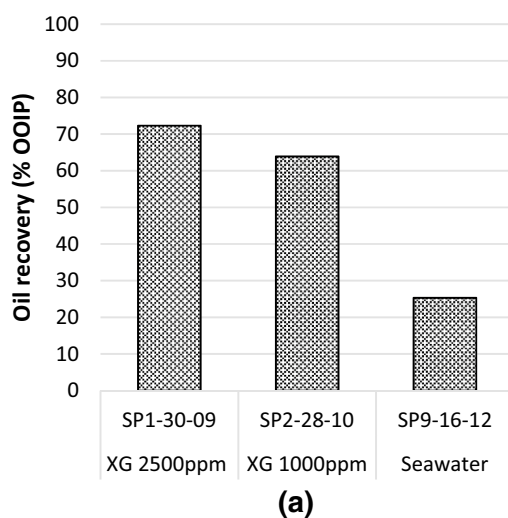


**Fig. 9** Oil recoveries from various sandpacks **a** motor oil and **b** heavy oil blend as the displaced fluids

recovery compared with the waterflood for the scenarios with the heavy oil blend being the displaced fluid.

The difference in oil recoveries for the different sandpacks can be attributed to the viscosity of the displacing fluids used within these experiments. In the waterflood scenarios, the viscosity of the displacing fluid was much less than that of the displaced fluid (motor oil and heavy oil blend), resulting in the lowest overall oil recovery. The XG 2500 ppm and XG 1000 ppm displacement fluids were more viscous than the seawater resulting in favourable displacement fronts, higher oil recovery and volumetric sweep efficiency.

While increasing polymer concentration led to an incremental increase in oil production through the improvement in volumetric sweep efficiency owing to mobility control, it is important to consider the impact of polymer rheology and particle plugging on injectivity and fracture growth [46, 47]. Additionally, according to Farajzadeh et al. [48] with an increase in polymer concentration, there is an increasing possibility of mechanical entrapment of the polymer molecules. Therefore, during the planning phase of any chemical, enhanced oil recovery operation, laboratory experiments should be conducted to determine and evaluate the polymer concentration in terms of operational (injectable flowrate), geomechanical (level of formation plugging and fracture-channelling) and economic feasibility needed to achieve the desired incremental hydrocarbon production and ultimate recovery [49].

## 4.2 History matching of flood pressure and oil production data

For the six polymer sandpack experiments in this study, the modified Corey-type analytical function was used in history matching the experimental data. Table 8 presents the Corey-type relative permeability parameters matched to the experimental data.

Figure 10 shows two experimental datasets of differential pressure and cumulative oil production with history

matching performed using the commercial software simulator Sendra. A reasonably good match was achieved between the experimental and simulation data. At the beginning of the flood experiments, the differential pressure in the flow system increased as the pressure of the injection fluid permeated through the sandpack corresponding to peak oil production with no displacing fluid being produced. After peak oil production, the differential pressure in the flow system gradually decreased with smaller amounts of oil being produced along with water or polymer; at this point, breakthrough has occurred. Initially, only oil (motor oil or heavy oil blend) was produced during the flooding operations, but as polymer breakthrough occurred both oil and polymer were produced. As the polymer flood experiments continued, the cumulative oil production stabilised.

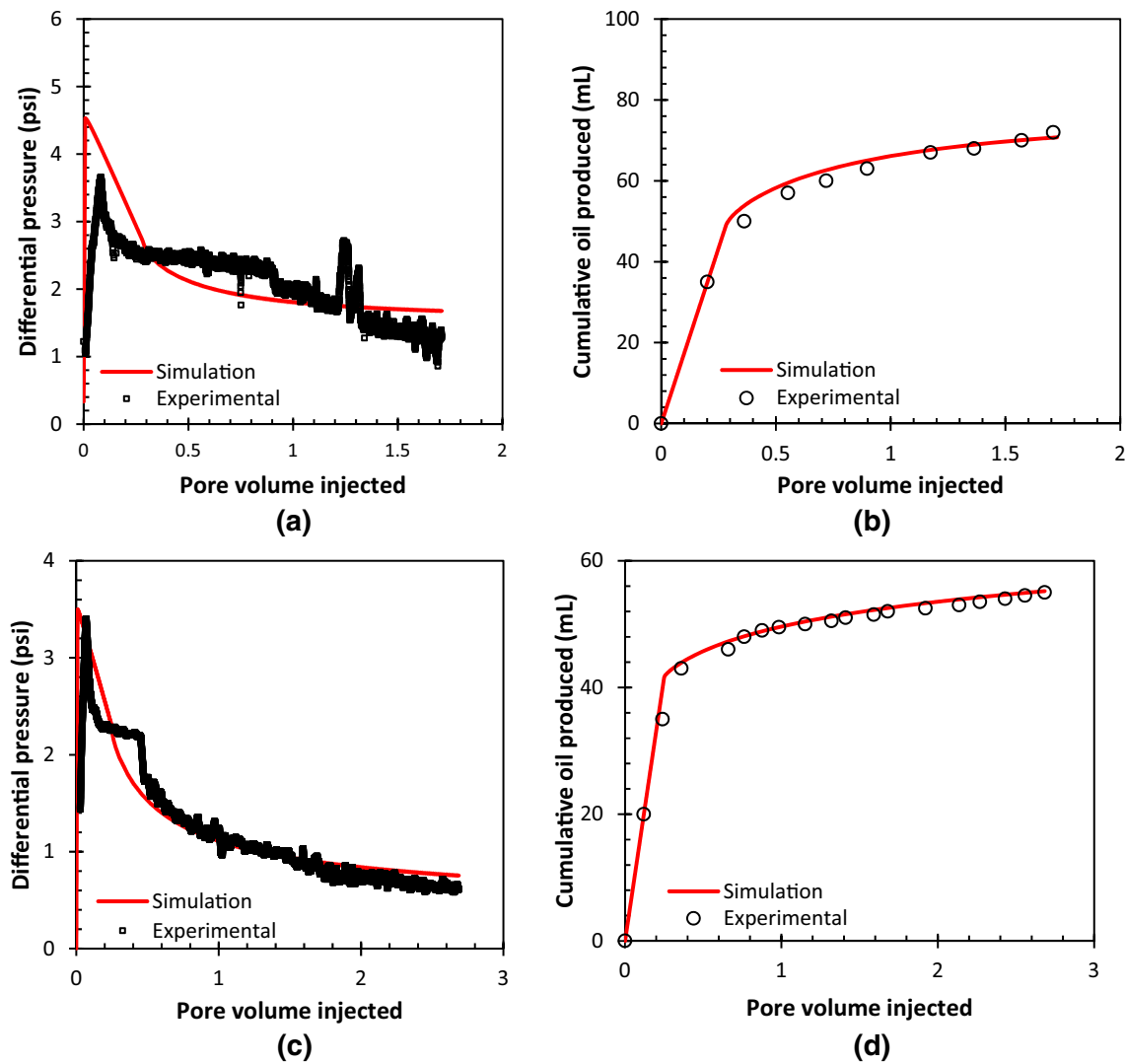
## 4.3 Effect of displacing fluid on relative permeability

Figure 11 shows the comparison of relative permeability curves of the six sandpack flood experiments using the Corey-type correlation relative permeability parameters matched to the experimental data from Table 8. The crossover point of the relative permeability curves provides insight into the wettability of the system under consideration. Wettability affects the relative location, flow and distribution of the fluids in the porous media. As such, a crossover point less than 0.5 represents a porous media which is oil-wet, whereas a crossover point greater than 0.5 represents a porous media which is water-wet. Oil-wet systems restrict the flow of oil and therefore result in lower oil recovery in contrast to water-wet systems which preferentially allow the flow of oil in larger pores as the oil blocks the flow of water [50, 51].

Figure 11a shows the comparison of the relative permeability curves for the cases of motor oil being the displaced fluid. As seen from the plot, the crossover point for the displacing fluid, seawater, was 0.46, 0.56 for the XG 1000 ppm polymer solution and 0.62 for the XG 2500 ppm polymer solution. It is observed that as the viscosity of the displacing fluid increases, there is a pronounced shift to the right of the crossover point of the relative permeability curves leading to a more favourable oil displacement condition as the volumetric sweep efficiency is enhanced [4]. Correspondingly, with an increase in the viscosity of the displacing fluid, there is an increase in the chemical concentration of the polymer solution which in turn affects the wettability condition of the porous media [3]. The observed change in the wettability condition of the sandpacks also enhances oil recovery due to induced changes in capillary pressure by means of the viscous forces at work [52]. Thus, the shift to the right of the crossover point of the relative

**Table 8** Corey correlation relative permeability parameters matched to experimental data

Sandpack	Oil type	Flooding fluid	Corey parameters	
			$N_w$	$N_o$
SP1-30-09	Motor oil	XG 2500 ppm	3.84	1.87
SP2-28-10	Motor oil	XG 1000 ppm	5.85	2.45
SP9-16-12	Motor oil	Seawater	3.15	2.30
SP7-02-12	Heavy oil blend	XG 2500 ppm	2.00	2.33
SP8-09-12	Heavy oil blend	XG 1000 ppm	2.31	2.05
SP10-18-12	Heavy oil blend	Seawater	4.86	4.11



**Fig. 10** Differential pressure and associated cumulative oil produced curves matched between experimental data and simulator for different sandpacks **a, b** SP8-09-16—heavy oil blend and XG 1000 ppm and **c, d** SP10-18-12—heavy oil blend and seawater

permeability curves is indicative of a change in the wettability condition of the porous media, with it becoming water-wet. Figure 11b presents the same comparison for the cases of the heavy oil blend being the displaced fluid. As observed from the plot, the crossover point for the displacing fluid seawater was 0.48, 0.53 for the XG 1000 ppm polymer solution and 0.54 for the XG 2500 ppm polymer solution. As such, a similar trend is observed with the displaced fluid being motor oil; as the viscosity of the displacing fluid increases the crossover point of the relative permeability curves shifts moderately to the right, resulting in a more favourable oil displacement condition. Similarly, with an increase in the chemical concentration of the polymer, there is indication of wettability changes in the condition of the porous media with a shift to the right of the crossover saturation, with the porous system becoming

water-wet. For both the motor oil and heavy oil blend being the displaced fluids, the results of the waterflood cases (water–oil systems) showed that the porous media exhibited oil-wet characteristics, while the polymer flood cases (polymer–oil systems) demonstrated water-wet characteristics. This is an evident demonstration of changes in the wettability condition of the porous media occurring due to the chemical concentration of the polymer solutions and the adsorption of polymer on the sand surface.

Strong parallelism is observed in terms of oil relative permeability in all cases with the displaced fluid being either motor oil or heavy oil blend, with a moderate effect on residual oil saturation. In the case of the motor oil being the displaced fluid (Fig. 11a), as the viscosity of the displacing fluid increased, its endpoint relative permeability decreased at a higher wetting saturation. However,

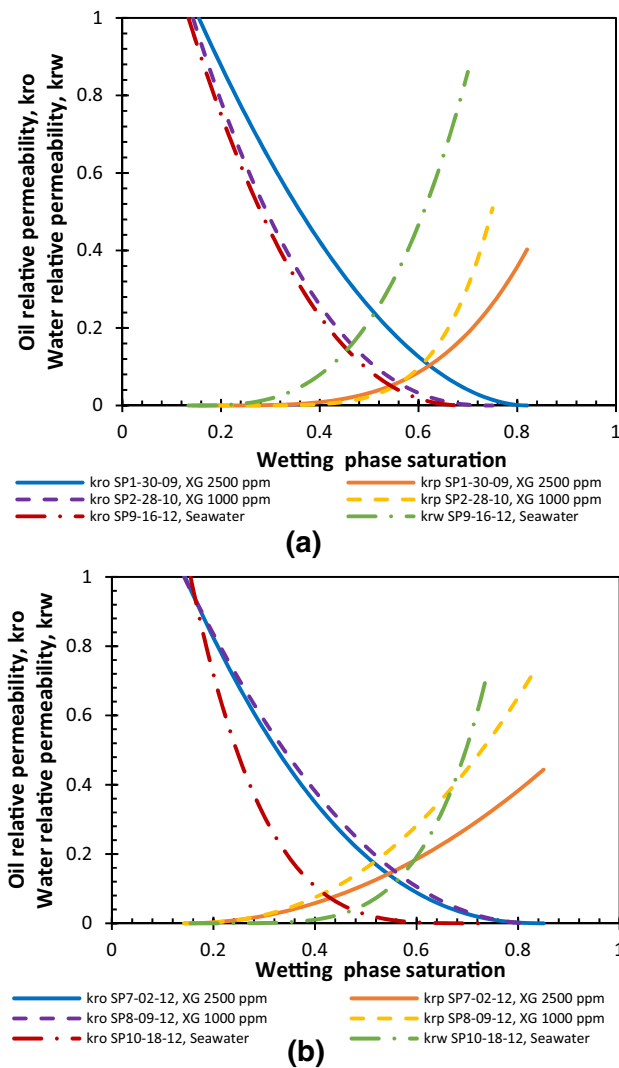


**Fig. 11** Relative permeability curves based upon experimental data for different sandpacks **a** motor oil and **b** heavy oil blend

in the case of the heavy oil blend being the displaced fluid (Fig. 11b), the XG 1000 ppm polymer solutions had a higher endpoint relative permeability than the seawater case but with the increasing viscosity of the displacing fluid, all cases exhibited higher wetting phase saturations. The difference in the shape of the relative permeability curves can be attributed to the lower viscosity of seawater to polymer solutions resulting in lower oil recovery. This phenomenon is indicative of the effect of mobility control of the seawater and different polymer concentrations.

#### 4.4 Effect of displacing fluid on fractional flow and saturation profile

Viscosity ratio is defined as the displaced fluid viscosity divided by the displacing fluid viscosity and influences

the main mechanism of polymer flooding. The increased viscosity of the polymer solution decreases the mobility of the displacing polymer solution to the displaced fluid resulting in reduced viscous fingering, thereby improving sweep efficiency, allowing the injected polymer to sweep the oil with a piston-like effect. When the mobility ratio is less than 1, the fractional flow curve is indicative of piston-like flow with the average wetting phase saturation having a larger value, resulting in better displacement efficiencies.

The mechanism of increased displacing fluid viscosity can be quantified using the Buckley–Leverett theory. Figure 12 presents the fractional flow curves of both the motor oil and heavy oil blend as the displaced fluids. In the cases of the motor oil being the displaced fluid (Fig. 12a), the viscosity ratio of the waterflood case had a water to oil ratio of 136, the polymer flood case with XG 1000 ppm polymer had a viscosity ratio of polymer to oil of 18, and the polymer flood case with XG 2500 ppm polymer had a viscosity ratio of polymer to oil of 9. In the cases of the heavy oil blend being the displaced fluid (Fig. 12b), the viscosity ratio of the waterflood case had a water to oil ratio of 156, the polymer flood case with XG 1000 ppm polymer had a viscosity ratio of polymer to oil of 20, and the polymer flood case with XG 2500 ppm polymer had a viscosity ratio of polymer to oil of 11.

From the fractional flow curve, the average water saturation at breakthrough was estimated by constructing a tangent from the irreducible water saturation ( $S_{wi}$ ) and intersecting the horizontal line of  $f_w = 1$ , which corresponds with the average water saturation. The  $f_w$  is the water cut in the producing fluid. In the cases of the motor oil being the displaced fluid (Fig. 12a), the average water saturation of the waterflood case was 0.31, the polymer flood case with XG 1000 ppm polymer was 0.58, and the polymer flood case with XG 2500 ppm is 0.66. The difference between the polymer flood cases of XG 2500 ppm and XG 1000 ppm were 0.35 and 0.27, respectively. In the cases of the heavy oil blend being the displaced fluid (Fig. 12b), the average water saturation of the waterflood case was 0.40, the polymer flood case with XG 1000 ppm polymer is 0.46, and the polymer flood case with XG 2500 ppm is 0.54. The difference between the polymer flood cases of XG 2500 ppm and XG 1000 ppm was 0.14 and 0.06, respectively. Thus, by increasing the viscosity of displacing fluid in the motor oil case, the oil recovery factor can be increased by a maximum 35% at breakthrough, whereas in the heavy oil blend case the oil recovery factor can be increased by a maximum 14% at breakthrough. In these flood experiments, it was seen that both the displaced fluid and displacing fluid viscosities impact the shape of the fractional flow curves considered in this study.

Figure 13 shows the saturation profiles for the three motor oil cases. It is observed that both water and polymer

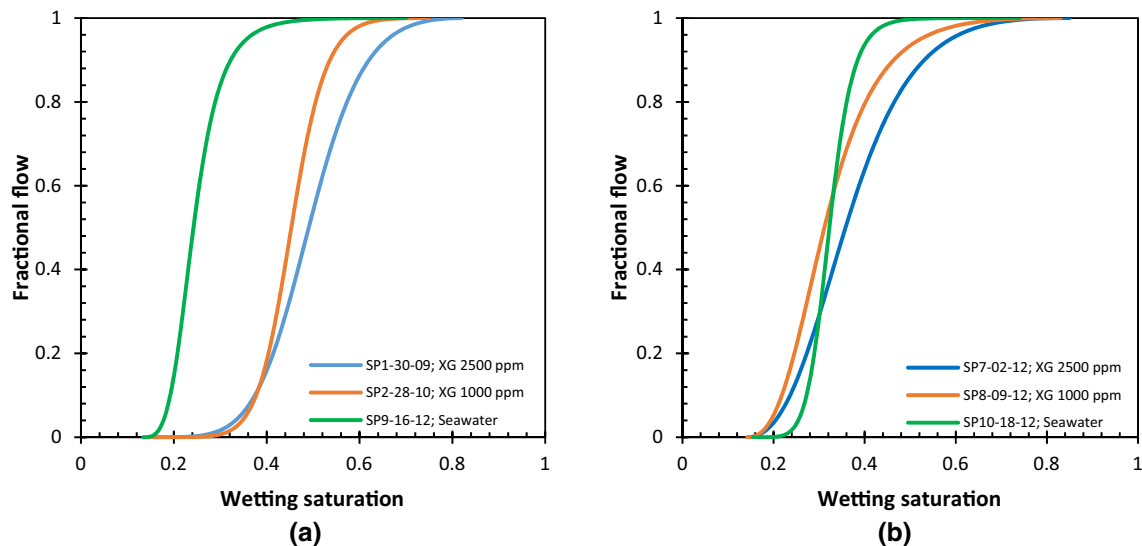


**Fig. 12** Fractional flow curves based upon experimental data for different sandpacks **a** motor oil and **b** heavy oil blend

fronts were formed through the porous media to differing degrees. These saturation profiles correspond to the breakthrough times of both the water and polymer solutions. Figure 13a represents the case where the displacing fluid is the XG 2500 ppm which had the longest polymer breakthrough at 0.58 PV (96 min). Figure 13b represents the case where the displacing fluid was the XG 1000 ppm which had a polymer breakthrough at 0.43 PV (70 min). Figure 13c represents the case where the displacing fluid was seawater which had the shortest water breakthrough at 0.13 PV (27 min). Increased oil recovery was achieved with delayed breakthrough times, 47.0% for the XG 2500 ppm compared to the waterflood and 38.6% for the XG 1000 ppm compared to the waterflood, indicative of improved mobility control. The oil and seawater have a larger contrast in their viscosity compared with the oil and polymer, thereby resulting in an unstable waterflood with strong viscous fingering. Thus, early water breakthrough was observed, due to the adverse viscosity ratio.

## 5 Conclusion and future perspective

In this study, displacement sequence experiments were used to investigate the effect of displaced fluid viscosity and displacing fluid viscosity on oil recovery in sandpacks. The displaced fluids were motor oil and a heavy oil blend, while the displacing fluids were seawater and xanthan polymer solutions, XG 2500 ppm and XG 1000 ppm. Relative permeabilities were estimated using the USS relative permeability method and employing the implicit history matching technique using the commercial simulator Sendra with the Corey-type analytical function. Results

showed that the high viscosity of the polymer solutions improves mobility control resulting in better sweep areas and displacement efficiencies. In the case of the motor oil displaced fluid, the XG 2500 ppm polymer achieved a 47.0% increase in oil recovery compared with the waterflood and the XG 1000 ppm polymer achieved a 38.6% increase in oil recovery compared with the waterflood. In the case of the heavy oil blend displaced fluid, the XG 2500 ppm polymer achieved a 44.8% increase in oil recovery compared with the waterflood and the XG 1000 ppm polymer achieved a 30.7% increase in oil recovery compared with the waterflood. Additionally, in the cases of the motor oil being the displaced fluid, the viscosity ratio was 136 for the waterflood case, 18 for the polymer flood case with XG 1000 ppm polymer and 9 for the polymer flood case with XG 2500 ppm polymer. In the cases of the heavy oil blend being the displaced fluid, the viscosity ratio was 156 for the waterflood case, 20 for the polymer flood case with XG 1000 ppm polymer and 11 for the polymer flood case with XG 2500 ppm polymer. The difference in the shape of the relative permeability curves and fractional flow curves were indicative of the effect of mobility control of each polymer concentration resulting in increased oil recovery compared to the waterflood cases. Experimental findings showed that for the waterflood cases (water–oil systems), the porous media exhibited oil-wet characteristics, while the polymer flood cases (polymer–oil systems) demonstrated water-wet characteristics for both the motor oil and heavy oil blend being the displaced fluids. Polymer adsorption on the sand surface of the porous media was inferred to be responsible for the changes in wettability condition. Saturation profiles showed that the oil and seawater had a larger contrast in their viscosity

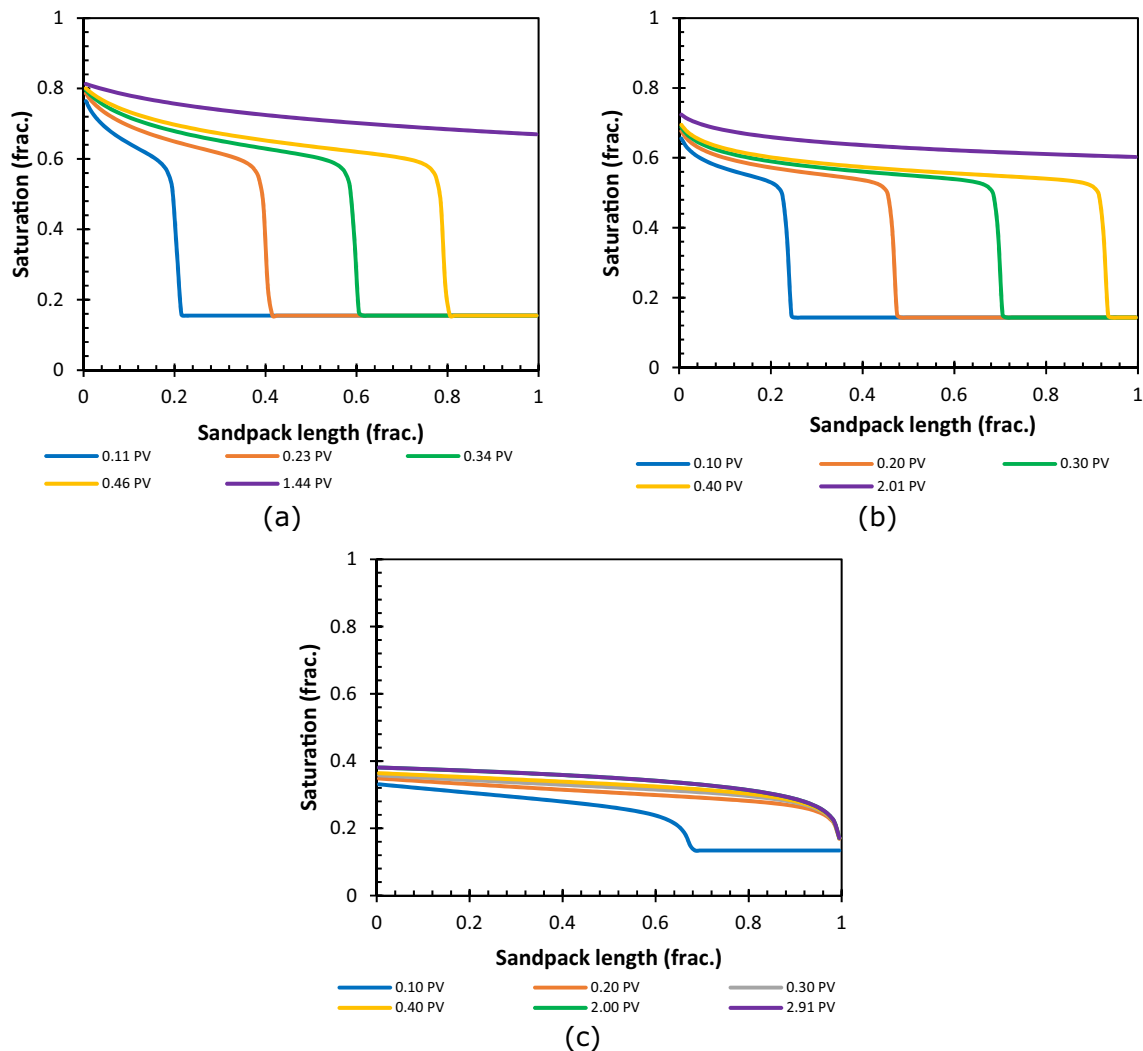


**Fig. 13** Saturation profile of motor oil cases along the sandpack column at varying PV intervals with the displacing fluid as **a** XG 2500 ppm, **b** XG 1000 ppm and **c** seawater

compared with the oil and polymer, thereby resulting in unstable waterflood with strong viscous fingering, leading to early water breakthrough due to the adverse viscosity ratio.

This study has provided further theoretical support of the potential of xanthan polymer to improve oil recovery and provides an insight into the mechanism behind oil displacement. Further laboratory research should be performed to investigate the effect of wettability, temperature, viscosity loss, polymer precipitation, optimal polymer concentration, time and injection rate.

**Acknowledgements** The authors are grateful to the School of Engineering at Robert Gordon University for facilitating and supporting this research work.

**Data availability** The datasets generated during and/or analysed during the current study are available from the corresponding author upon request.

### Compliance with ethical standards

**Conflict of interest** The authors declare that there is no conflict of interest.

**Open Access** This article is licensed under a Creative Commons Attribution 4.0 International License, which permits use, sharing, adaptation, distribution and reproduction in any medium or format, as long as you give appropriate credit to the original author(s) and the source, provide a link to the Creative Commons licence, and indicate if changes were made. The images or other third party material in this article are included in the article's Creative Commons licence, unless indicated otherwise in a credit line to the material. If material is not included in the article's Creative Commons licence and your intended use is not permitted by statutory regulation or exceeds the permitted use, you will need to obtain permission directly from the copyright

holder. To view a copy of this licence, visit <http://creativecommons.org/licenses/by/4.0/>.

## References

1. Sönnichsen N (2020) Global energy consumption by energy source 1990–2040. New York, United States
2. Ding L, Wu Q, Zhang L, Guérillot D (2020) Application of fractional flow theory for analytical modeling of surfactant flooding, polymer flooding, and surfactant/polymer flooding for chemical enhanced oil recovery. *Water* 12(8):1–29. <https://doi.org/10.3390/w12082195>
3. Gbadamosi AO, Junin R, Manan MA, Agi A, Yusuff AS (2019) An overview of chemical enhanced oil recovery: recent advances and prospects. *Int Nano Lett* 9(3):171–202. <https://doi.org/10.1007/s40089-019-0272-8>
4. Li Z, Ayirala S, Mariath R, AlSofi A, Xu Z, Yousef A (2020) Micro-scale effects of polymer on wettability alteration in carbonates. *SPE J*. <https://doi.org/10.2118/200251-PA>
5. Firozjahi AM, Zargar G, Kazemzadeh E (2019) An investigation into polymer flooding in high temperature and high salinity oil reservoir using acrylamide based cationic co-polymer: experimental and numerical simulation. *J Pet Explor Prod Technol* 9(2):1485–1494. <https://doi.org/10.1007/s13202-018-0557-x>
6. Zhong H, Li Y, Zhang W, Li D (2019) Study on microscopic flow mechanism of polymer flooding. *Arab J Geosci* 12(56):1–10. <https://doi.org/10.1007/s12517-018-4210-2>
7. Delamaide E (2016) Comparison of primary, secondary and tertiary polymer flood in heavy oil – field results. In: *SPE Trinidad Tobago Sect. Energy Resour. Conf. SPE, Port of Spain, Trinidad and Tobago*, pp 1–20
8. Yegin C, Singh BP, Zhang M et al (2017) Next-generation displacement fluids for enhanced oil recovery. In: *SPE Oil Gas India Conf. Exhib. SPE, Mumbai, India*, pp 1–29
9. Manrique E, Ahmadi M, Samani S (2017) Historical and recent observations in polymer floods: an update review. *CT&F - Ciencia, Tecnol y Futur* 6(5):17–48. <https://doi.org/10.29047/01225383.72>
10. Mohajeri M, Hemmati M, Shekarabi AS (2015) An experimental study on using a nanosurfactant in an EOR process of heavy oil in a fractured micromodel. *J Pet Sci Eng* 126:162–173. <https://doi.org/10.1016/j.petrol.2014.11.012>
11. Schneider FN, Owens WW (1982) Steady-state measurements of relative permeability for polymer/oil systems. *Soc Pet Eng J* 22(1):79–86. <https://doi.org/10.2118/9408-PA>
12. Abirov R, Ivakhnenko AP, Abirov Z, Eremin NA (2020) The associative polymer flooding: an experimental study. *J Pet Explor Prod Technol* 10:447–454. <https://doi.org/10.1007/s13202-019-0696-8>
13. Al-Shakry B, Shiran BS, Skauge T, Skauge A (2018) Enhanced oil recovery by polymer flooding: optimizing polymer injectivity. In: *SPE Kingdom Saudi Arab. Annu. Tech. Symp. Exhib. SPE, Dammam, Saudi Arabia*, pp 1–22
14. Song Z, Liu L, Wei M, Bai B, Hou J, Li Z, Hu Y (2015) Effect of polymer on disproportionate permeability reduction to gas and water for fractured shales. *Fuel* 143:28–37. <https://doi.org/10.1016/j.fuel.2014.11.037>
15. Fabbri C, de Loubens R, Skauge A, Ormehaug PA, Vik B, Bourgeois M, Morel D, Hamon G (2015) Comparison of history-matched water flood, tertiary polymer flood relative permeabilities and evidence of hysteresis during tertiary polymer flood in very viscous oils. In: *SPE Asia Pacific Enhanc. Oil Recover. Conf. SPE, Kuala Lumpur, Malaysia*, pp 1–19
16. Lopez X, Blunt MJ (2004) Predicting the impact of non-Newtonian rheology on relative permeability using porescale modeling. In: *SPE Annu. Tech. Conf. Exhib. SPE, Houston, Texas, USA*, pp 1–8
17. Barreau P, Lasseux D, Bertin H, Glenat P, Zaitoun A (1999) An experimental and numerical study of polymer action on relative permeability and capillary pressure. *Pet Geosci* 5(2):201–206. <https://doi.org/10.1144/petgeo.5.2.201>
18. Ashrafi M, Souraki Y, Torsaeter O (2014) Investigating the temperature dependency of oil and water relative permeabilities for heavy oil systems. *Transp Porous Media* 105:517–537. <https://doi.org/10.1007/s11242-014-0382-8>
19. Alhammad AM, Gao Y, Akai T, Blunt MJ, Bijeljic B (2020) Porescale X-ray imaging with measurement of relative permeability, capillary pressure and oil recovery in a mixed-wet micro-porous carbonate reservoir rock. *Fuel* 268:117018. <https://doi.org/10.1016/j.fuel.2020.117018>
20. Doranehgard MH, Siavashi M (2018) The effect of temperature dependent relative permeability on heavy oil recovery during hot water injection process using streamline-based simulation. *Appl Therm Eng* 129:106–116. <https://doi.org/10.1016/j.applthermaleng.2017.10.002>
21. Arigbe OD, Oyeneyin MB, Arana I, Ghazi MD (2019) Real-time relative permeability prediction using deep learning. *J Pet Explor Prod Technol* 9(2):1271–1284. <https://doi.org/10.1007/s13202-018-0578-5>
22. Liu Y, Hou J, Liu L, Zhou K, Zhang Y, Dai T, Guo L, Cao W (2018) An inversion method of relative permeability curves in polymer flooding considering physical properties of polymer. *SPE J* 23(5):1929–1943. <https://doi.org/10.2118/189980-PA>
23. Hou J, Wang D, Luo F, Li Z, Bing S (2012) Estimation of the water–oil relative permeability curve from radial displacement experiments. Part 1: numerical inversion method. *Energy & Fuels* 26(7):4291–4299. <https://doi.org/10.1021/ef300018w>
24. Schembre JM, Kovscek AR (2006) Estimation of dynamic relative permeability and capillary pressure from countercurrent imbibition experiments. *Transp Porous Media* 65(1):31–51. <https://doi.org/10.1007/s11242-005-6092-5>
25. Fayazi A, Bagherzadeh H, Shahrabadi A (2016) Estimation of pseudo relative permeability curves for a heterogeneous reservoir with a new automatic history matching algorithm. *J Pet Sci Eng* 140:154–163. <https://doi.org/10.1016/j.petrol.2016.01.013>
26. Zhang Y, Song C, Yang D (2016) A damped iterative EnKF method to estimate relative permeability and capillary pressure for tight formations from displacement experiments. *Fuel* 167:306–315. <https://doi.org/10.1016/j.fuel.2015.11.040>
27. Zhang Y, Yang D (2013) Simultaneous estimation of relative permeability and capillary pressure for tight formations using ensemble-based history matching method. *Comput Fluids* 71:446–460. <https://doi.org/10.1016/j.compfluid.2012.11.013>
28. Li H, Chen SN, Yang D (Tony), Tontiwachwuthikul P (2012) Estimation of relative permeability by assisted history matching using the Ensemble Kalman Filter method. *J Can Pet Technol* 51(3):2012. <https://doi.org/10.2118/156027-PA>
29. Eydinov D, Gao G, Li G, Reynolds AC (2009) Simultaneous estimation of relative permeability and porosity/permeability fields by history matching production data. *J Can Pet Technol* 48(12):13–25. <https://doi.org/10.2118/132159-PA>
30. Sun X, Mohanty KK (2005) Estimation of flow functions during drainage using genetic algorithm. *SPE J* 10(4):449–457. <https://doi.org/10.2118/84548-PA>
31. Giller B, Ertekin T, Grader AS (1999) An artificial neural network based relative permeability predictor. In: *Tech. Meet. / Pet. Conf. South Saskatchewan Sect. Petroleum Society of Canada*, pp 1–25

32. Yang PH, Watson AT (1991) A Bayesian methodology for estimating relative permeability curves. *SPE Reserv Eng* 6(2):259–265. <https://doi.org/10.2118/18531-PA>
33. Bai M, Liu L, Li C, Song K (2020) Relative permeability characteristics during carbon capture and sequestration process in low-permeable reservoirs. *Materials (Basel)* 13(4):1–15. <https://doi.org/10.3390/ma13040990>
34. Parvazdavani M, Abbasi S, Zare-Reisabadi M (2017) Experimental study of gas–oil relative permeability curves at immiscible/near miscible gas injection in highly naturally fractured reservoir. *Egypt J Pet* 26(1):171–180. <https://doi.org/10.1016/j.ejpe.2016.01.002>
35. Johnson EF, Bossler DP, Bossler VON (1959) Calculation of relative permeability from displacement experiments. *Trans AIME* 216:370–372. <https://doi.org/10.2118/1023-G>
36. Jones SC, Roszelle WO (1978) Graphical techniques for determining relative permeability from displacement experiments. *J Pet Technol* 30:807–817. <https://doi.org/10.2118/6045-PA>
37. Sendra (2018) *Sendra User Guide 2018.2*. Norway
38. Corey A (1954) The interrelation between gas and oil relative permeabilities. *Prod Mon* 38–41
39. Sigmund PM, McCaffery FG (1979) An improved unsteady-state procedure for determining the relative-permeability characteristics of heterogeneous porous media (includes associated papers 8028 and 8777). *Soc Pet Eng J* 19(1):15–28. <https://doi.org/10.2118/6720-PA>
40. Lomeland F, Ebeltoft E, Thomas WH (2005) A new versatile relative permeability correlation. In: *Int. Symp. Soc. Core Anal.* Toronto, Canada, pp 1–12
41. Burdine NT (1953) Relative permeability calculations from pore size distribution data. *J Petrol Technol* 5(3):71–78. <https://doi.org/10.2118/225-G>
42. Chierici GL (1984) Novel relations for drainage and imbibition relative permeabilities. *Soc Pet Eng J* 24(3):275–276. <https://doi.org/10.2118/10165-PA>
43. Esmaeili S, Sarma H, Harding T, Maini B (2019) Correlations for effect of temperature on oil/water relative permeability in clastic reservoirs. *Fuel* 246:93–103. <https://doi.org/10.1016/j.fuel.2019.02.109>
44. Mosavat N, Torabi F, Zarivnyy O (2013) Developing new Corey-based water/oil relative permeability correlations for heavy oil systems. In: *SPE Heavy Oil Conf.* SPE, Calgary, Alberta, Canada, pp 1–18
45. Firozjii AM, Saghafi HR (2020) Review on chemical enhanced oil recovery using polymer flooding: fundamentals, experimental and numerical simulation. *Petroleum*. <https://doi.org/10.1016/j.petlm.2019.09.003>
46. Zechner M, Clemens T, Suri A, Sharma MM (2015) Simulation of polymer injection under fracturing conditions—An injectivity pilot in the Matzen Field, Austria. *SPE Reserv Eval Eng* 18(2):236–249. <https://doi.org/10.2118/169043-PA>
47. Seright RS (2017) How much polymer should be injected during a polymer flood? Review of previous and current practices. *SPE J*. <https://doi.org/10.2118/179543-PA>
48. Farajzadeh R, Wassing BL, Lake LW (2019) Insights into design of mobility control for chemical enhanced oil recovery. *Energy Reports* 5:570–578. <https://doi.org/10.1016/j.egy.2019.05.001>
49. Mahon R, Balogun Y, Oluyemi G, Njuguna J (2020) Swelling performance of sodium polyacrylate and poly(acrylamide-co-acrylic acid) potassium salt. *SN Appl Sci*. <https://doi.org/10.1007/s42452-019-1874-5>
50. Tarek A (2019) *Reservoir Engineering Handbook*. <https://doi.org/10.1016/C2016-0-04718-6>
51. Wheaton R (2016) *Fundamentals of Applied Reservoir Engineering*. <https://doi.org/10.1016/C2015-0-04617-2>
52. El-hoshoudy AN, Desouky SEM, Elkady MY, Al-Sabagh AM, Betiha MA, Mahmoud S (2017) Hydrophobically associated polymers for wettability alteration and enhanced oil recovery – Article review. *Egypt J Pet* 26:757–762. <https://doi.org/10.1016/j.ejpe.2016.10.008>

**Publisher's Note** Springer Nature remains neutral with regard to jurisdictional claims in published maps and institutional affiliations.